VU Research Portal

Flexibility and size heterogeneity of the LH1 light harvesting complex revealed by atomic force microscopy - Functional significance for bacterial photosynthesis

Bahatyrova, S.; Frese, R.N.; van der Werf, K.O.; Otto, C.; Hunter, C.N.; Olsen, J.D.

document version
Publisher's PDF, also known as Version of record

Link to publication in VU Research Portal

Flexibility and Size Heterogeneity of the LH1 Light Harvesting Complex Revealed by Atomic Force Microscopy

FUNCTIONAL SIGNIFICANCE FOR BACTERIAL PHOTOSYNTHESIS*⑤

Svetlana Bahatyrova‡, Raoul N. Frese‡§, Kees O. van der Werf‡, Cees Otto‡, C. Neil Hunter¶‖, and John D. Olsen¶

From the ‡Biophysical Techniques Group, Department of Science and Technology, University of Twente, 7500 AE Enschede, The Netherlands and ¶Robert Hill Institute for Photosynthesis Research, Krebs Institute for Biomolecular Research, Department of Molecular Biology and Biotechnology, University of Sheffield, Sheffield S10 2TN, United Kingdom

Previous electron microscopic studies of bacterial RC-LH1 complexes demonstrated both circular and elliptical conformations of the LH1 ring, and this implied flexibility has been suggested to allow passage of quinol from the Q_B site of the RC to the quinone pool prior to reduction of the cytochrome bc_1 complex. We have used atomic force microscopy to demonstrate that these are just two of many conformations for the LH1 ring, which displays large molecule-to-molecule variations, in terms of both shape and size. This atomic force microscope study has used a mutant lacking the reaction center complex, which normally sits within the LH1 ring providing a barrier to substantial changes in shape. This approach has revealed the inherent flexibility and lack of structural coherence of this complex in a reconstituted lipid bilayer at room temperature. Circular, elliptical, and even polygonal ring shapes as well as arcs and open rings have been observed for LH1; in contrast, no such variations in structure were observed for the LH2 complex under the same conditions. The basis for these differences between LH1 and LH2 is suggested to be the H-bonding patterns that stabilize binding of the bacteriochlorophylls to the LH polypeptides. The existence of open rings and arcs provides a direct visualization of the consequences of the relatively weak associations that govern the aggregation of the protomers $(\alpha_1\beta_1Bchl_2)$ comprising the LH1 complex. The demonstration that the linkage between adjacent protomer units is flexible and can even be uncoupled at room temperature in a detergent-free membrane bilayer provides a rationale for the dynamic separation of individual protomers, and we may now envisage experiments that seek to prove this active opening process.

Photosynthetic organisms harvest light energy and convert it to a chemically useful form, using light harvesting (LH)[1] and reaction center (RC) complexes. In the purple photosynthetic bacteria, the reaction center, which is the site of photochemistry, receives excitation energy from the light harvesting LH1 complex, which receives energy in turn from the LH2 complex (reviewed in Ref. 1). The atomic structure of the *Rhodopseudomonas acidophila* LH2 complex (2) and the cryo-electron microscopy (EM) structure of the *Rhodobacter sphaeroides* complex (3) both revealed a circular arrangement of nine protomers, each consisting of an α and a β polypeptide. The LH2α polypeptides formed an inner ring, with the β ring outermost; in all, 27 bacteriochlorophyll (Bchl) molecules are bound to this structure (2). More recent work has established that LH1 surrounds the RC using an arrangement of 16 αβ protomers and 32 Bchls (4) when there is no prulifloxacin PufX protein. In other bacteria, an LH1 ring of 15 αβ protomers, together with either PufX or a putative PufX homologue (W), form a continuous ring of protein around the RC (5, 6). The demonstration of both circular and elliptical forms of this LH1 complex provided evidence for its flexibility (4). This property of the LH1 complex was suggested to be a significant factor in the export of quinol, the product of RC photochemistry, to the cytochrome bc_1 complex (4). For organisms such as *Rhodospirillum rubrum*, which assemble an $(\alpha\beta)_{16}$ LH1 complex completely enclosing the RC, such flexibility would clearly be an essential feature of this LH complex and would imply a dynamic series of conformations *in vivo*. However, only the extremes of this dynamic population have been reported, and the flexibility hypothesis requires the imaging of several conformations at room temperature.

For other photosynthetic bacteria such as *R. sphaeroides*, *Rhodobacter capsulatus*, and *Rhodopseudomonas palustris* other possibilities for quinol export became apparent when it was found that these bacteria assemble another polypeptide, PufX (W), into the LH1 complex. It was discovered that *puf* X⁻ mutants were unable to photosynthesize (7, 8); subsequently, such mutants were found to be impaired in their ability to shuttle quinones/quinols in and of the Q_B site of the RC (9, 10). It was suggested that PufX forms part of the LH1 ring, providing a portal for quinol (11). This concept would seem to be supported by work on mutants with an LH1 complex that is too small to completely surround the RC; these mutants can, therefore, allow free movement of quinones/quinols to the RC Q_B site, and so they are fully capable of photosynthetic growth, even in the absence of PufX (12). Studies on RC-LH1-PufX complexes in native membranes show that PufX causes a spe-

---

[1] The abbreviations used are: LH, light harvesting; RC, reaction center; Bchl, bacteriochlorophyll; AFM, atomic force microscope; EM, electron microscopy.

cific orientation of the RC, which is the likely cause of the long range organization of the core complexes (6, 13) and plays a role in organizing the core complex into dimers in detergent-solubilized systems (14, 15).

It is not known whether the LH1 complex of *R. sphaeroides* is flexible, and if so, to what extent; perhaps there is no need if PufX does indeed provide a quinol portal. In terms of LH1 flexibility, we are confined at present to the knowledge, based upon cryo-electron microscopy studies of two-dimensional crystals, that the *R. rubrum* LH1 complex lacking PufX can assume both circular and elliptical forms. This observation is subject to the limitations that the crystals are frozen in glucose at ~77 K and that LH1 molecules in disordered regions will not be represented. The use of the atomic force microscope (AFM) to image the surface of two-dimensional crystals presents us with the opportunity to obtain high signal-to-noise data without the need for processing the data, and particularly without the need to obtain large, highly ordered crystals. Previous studies have amply illustrated the usefulness of AFM for imaging two-dimensional crystals of the LH2 complexes of *Rubrivivax gelatinosus* (16), *R. sphaeroides* (17), and *R. acidophila* (18). Scheuring *et al.* (19) achieved the imaging of native membranes of *Blastochloris viridis* containing RC-LH1 complexes by AFM and were able to show that LH1 formed an ellipse round the RC, but that it became circular upon removal of the RC.

In view of the possible functional significance of alterations in conformation of the LH1 ring, it is important to visualize all of the possible shapes and aggregation states of which LH1 is capable. This should be compared with the peripheral LH2 complex, using the same methodology. Scheuring *et al.* (17) have extensively characterized large planar two-dimensional crystals of the LH2 complex from *R. sphaeroides* by AFM. In our work, we have examined different crystal forms of the LH2 complex, to establish whether alterations in crystal packing produce distortions of the LH2 complex. In this regard, it is already known that lateral packing forces exerted in two-dimensional crystals can distort RC-LH1 complexes into circles or ellipses, depending on whether the crystal form is tetragonal or orthorhombic, respectively (4). Recently, high-resolution AFM was used to image two-dimensional crystals of the RC-LH1 complex of *R. rubrum* (20). It was shown that the RC-LH1 complex may adopt an irregular shape in regions of uneven packing forces in the crystal, reflecting a likely flexibility when in the natural membrane. This study also imaged a few LH1-only complexes, formed as a consequence of removing the RC with the AFM tip, which showed some of the possibilities for distorting this complex. To examine this in more detail, it is important to obtain images of many LH1 complexes free of the RC; it is only then that the inherent flexibility and even deformability of LH1 will be revealed, because the RC, which sits fairly tightly within the LH1 ring, normally provides a barrier to substantial deformation.

We have used AFM to compare two-dimensional crystals of LH1 and of LH2 of *R. sphaeroides*. We find that the LH2 crystals have three different packing forms and despite the differing packing forces, the complexes are essentially always circular. In contrast, LH1 molecules displayed a wide range of both ring sizes and packing geometries that generated circular, elliptical, and even polygonal ring shapes as well as arcs and open rings. From these data, we conclude that the LH1 ring is intrinsically highly deformable, and we relate this property to the manner in which it is assembled and further to its operation within the photosynthetic unit.

EXPERIMENTAL PROCEDURES

Materials—All chemicals were purchased from Sigma (Poole, UK) except the detergent β-OG (*n*-octyl β-D-glucopyranoside), which was

obtained from Calbiochem (Merck Biosciences, Nottingham, UK) and the lipid DOPC (1,2-dioleoyl-sn-glycero-3-phosphocholine), which was obtained from Avanti Polar Lipids (Alabaster, AL). All chemicals were of Analar or equivalent grade.

Isolation and Purification of LH1 and LH2 Complexes

Strains and Plasmids—The *R. sphaeroides* strains used have all been described previously: DD13, LH2⁻ LH1⁻ RC⁻ (21); DPF2, LH2-only (21); *E. coli* S17–1 (22); DD13(pRKEK1), LH1-only (21).

The LH2-only strain DPF2 was grown semi-aerobically, and the intracytoplasmic membranes were prepared according to the methods in Olsen *et al.* (23). The plasmid pRKEK1 was introduced into the double-deletion strain DD13 by conjugative transfer. Colonies were examined for the presence of the LH1 wild-type complex using a Guided Wave 260 fiber-optic spectrophotometer and a home-built plate holder. Representative colonies were then grown semi-aerobically in liquid culture, and intracytoplasmic membranes were isolated as described previously (23), except that in this work we used a lower growth temperature of 30 °C and then concentrated the membranes by centrifugation at 186,000 × *g* for 4.5 h after diluting the sucrose present to less than 5%, prior to LH purification.

Two-dimensional Crystallization—LH2 was purified and crystallized as described in Waltz *et al.* (3). For LH1, ~500 absorbance units of concentrated LH1-only membrane sample were solubilized with 1.5 ml of 20% β-OG with gentle stirring at 10 °C and then loaded onto a pre-equilibrated 15-ml DEAE column. The column was washed for an hour at a flow rate of 1 ml/min with 155 mM NaCl, 10 mM Tris, pH 7.5, 1% β-OG, then eluted with a 155–400 mM NaCl salt gradient over 60 min at 1 ml/min. The best fractions were determined by the ratio of the absorbance at ~850 nm *versus* 280 nm, and these were used for two-dimensional crystallization trials using the lipid DOPC.

Atomic Force Microscopy and Image Processing—Muscovite mica purchased from Ted Pella (Redding, CA) was chosen as a support for the samples. For AFM measurements, the sample of LH2 crystals was prepared by adsorbing 1 μl of sample solution onto the surface of freshly cleaved mica for ~30 s, then the sample was immersed into the distilled and filtered water for 1 min to remove weakly bound crystal patches. The sample was immediately placed onto the AFM stage, and 300 μl of recording buffer (10 mM Tris-HCl, pH 7.5, 150 mM KCl) was added to the liquid cell. For firm attachment of LH1 crystals, the adsorption buffer (10 mM Tris-HCl, pH 7.5, 150 mM KCl, 25 mM MgCl₂) was applied, and the adsorption time was increased to 1 h. The imaging buffer used was the same as for the LH2 crystals.

For the experiments, a home-built stand-alone AFM was employed (24). Standard silicon nitride cantilevers with a length of 85 μm, force constant of 0.5 N·m, and operating frequencies of 25–35 kHz (in liquid) purchased from ThermoMicroscopes (Sunnyvale, CA) were used. High-resolution AFM images were obtained using tapping mode in liquid with a free amplitude of 2–5 nm; the amplitude setpoint was adjusted to minimal forces (damping of the free amplitude was 10–20%). Images contained 256 × 256 pixels and were recorded at a line frequency of 2–4 Hz. The calibration of the setup was made with UltraSharp Calibration Gratings from NT-MDT (Moscow, Russia). Topographical images were quantitatively analyzed by means of Scanning Probe image processor program (Image Metrology ApS, Lyngby, Denmark). All the images presented here were processed by applying a low-pass filter and are represented in three-dimensional view, unless otherwise specified.

RESULTS

Morphology of Two-dimensional Crystals Formed from LH1 Complexes: Comparison with LH2 Crystals—The "empty" LH1 complex containing no RC formed a homogeneous population of planar single-layered crystals between 100 and 700 nm in width (an example of a crystal ~300 nm in diameter is shown in Fig. 1*A*). The height of the crystals above the mica surface was 6.7 ± 0.4 nm, (*n* = 81; Table I, supplemental material). Most of the LH1 crystals displayed dense packing of LH1 complexes, whereas some of the crystals also contained empty areas of lipid bilayer with an average height above the mica surface of 4.1 ± 0.2 nm, *n* = 20 (Table I, supplemental material). In contrast, tubular crystals (Fig. 1*B*) were found most frequently for the LH2 complex, some of which had ruptured, forming single-layered sheets up to 1 μm wide. Intact tubes could be distinguished from the single-layered sheets (open

FIG. 1. **Examples of LH1 and LH2 two-dimensional crystals.** *A*, LH1 crystal: frame size, 500 × 500 nm²; full gray-scale, 11 nm. *B*, LH2 tubular crystals: frame size, 11 × 11 μm²; full gray-scale, 13 nm. *C*, LH2 vesicular crystals: frame size, 500 × 500 nm²; full gray-scale, 25 nm. The images represent raw, unprocessed data.

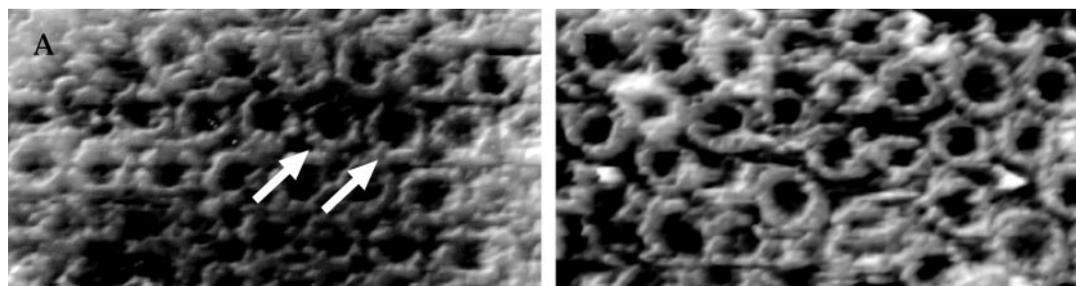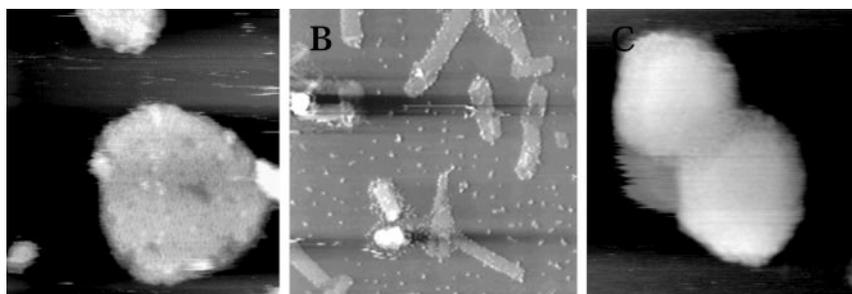FIG. 2. **Variations in packing for LH1 crystals.** *A*, ordered (hexagonal): frame size, 65 × 130 nm²; full gray-scale, 1.8 nm. *B*, disordered packing: frame size, 65 × 130 nm²; full gray-scale, 3.2 nm. The *right* and *left arrows* indicate large and small LH1 complexes, respectively.

tubes) also by analyzing their average height above the mica surface. The height histogram of the accumulated data showed two peaks in the height distribution, 7.2 ± 3.2 nm and 16 ± 2.4 nm ($n = 62$), corresponding to single-layered sheets and double-layered intact tubular crystals, respectively. Empty lipid patches were also observed for LH2 crystals, with an average height of 4.1 ± 0.1 nm ($n = 16$), which corresponds well with the number obtained from the analysis of LH1 crystals. Vesicular LH2 crystals (Fig. 1*C*) were observed less frequently and consisted of small round patches (average diameter ∼ 200 nm). The average height of the vesicular two-dimensional crystals was 15.9 ± 0.8 nm ($n = 11$).

Variations in Packing in Two-dimensional Crystals—The different packing arrangements of LH1-only complexes are shown in Fig. 2, *A* and *B*). No long range crystalline ordering was observed for LH1, unlike the situation for LH2 (Fig. 3; Refs. 3 and 17). In rare cases, LH1 rings formed small areas of well ordered crystalline lattices with a tentative assignment of hexagonal packing (Fig. 2*A*). This could only be observed in vesicles of larger than average size, *i.e.* more than 500 nm. This ordering was also accompanied by a marked preference for a single orientation, as determined by the height of the protruding face of the complex (see Table II, supplemental material). The majority of LH1 rings (86%) were positioned in the lipid membrane in the "down" orientation, characterized by a height from the lipid surface to the highest point of LH1 of 0.8 ± 0.1 nm ($n = 261$). In the opposite orientation, this height is 1.4 ± 0.1 nm ($n = 43$). It should be emphasized that LH1 rings, which tended to be circular in the well ordered areas of crystals (see Fig. 2*A*), still displayed some heterogeneity in size. For example, the *left* and *right arrows* in Fig. 2*A* indicate ring sizes of 12.6 and 14.1 nm, respectively. The high level of disorder of LH1 aggregates typified by Fig. 2*B* was accompanied by heterogeneity of the LH1 complexes in terms of differing ring sizes, with each size category displaying at least two different shapes. Broken rings and also incomplete arcs were found.

Crystalline packing of LH2 complexes was clearly resolved, and AFM images indicated that this fell into three categories; type A, a zigzag pattern; type B, a rectangular pattern; and type C, disordered. These are displayed separately in Fig. 3; in Fig. 3*D*, it can be seen that all three types of packing could be

found within one crystal. A Fourier transform of AFM images of type A crystals directly allowed the definition of a unit cell (a = 19.9 nm, b = 15.9 nm, γ = 87°). The unit cell encompasses four LH2 rings, two facing upwards and two downwards, which are clearly resolved. One face of the complex protrudes more than the other; the height from the lipid surface to the extremity of LH2 ("up") was 1.0 ± 0.1 nm ($n = 105$), and in the opposite orientation ("down"), this was 0.5 ± 0.1 nm ($n = 96$). This up-down configuration has been reported before from two-dimensional EM data (3) and from subsequent AFM studies on LH2 two-dimensional-crystals (16, 17). The primary difference between type B and type A crystal packing is that in the former, there is no close contact between adjacent up rings in the unit cell, whereas in type A, they are brought together very closely. Type C crystals do not show any distinct periodical pattern (Fig. 3*C*), as the LH2 complexes are incorporated into the lipid bilayer in a random, chaotic way. We could not resolve any up-down configuration in this case, but the distance between the up LH2 molecules provides enough space for oppositely oriented rings.

Detailed Characteristics of LH1 and LH2 Rings—Fig. 4*A* shows a high-resolution image of LH1 complexes embedded in a representative, disordered two-dimensional crystal. LH1 complexes displayed a high level of heterogeneity in shapes, sizes, and conformation. In contrast, LH2 complexes showed no such heterogeneity. Fig. 4, *B* and *C* show high magnification images of LH2 rings. The most noteworthy finding was that under no circumstances, not even for disordered regions of two-dimensional crystals, did the LH2 complex display the heterogeneity in size and shape we observed for LH1. Regardless of the type of packing or disorder, all LH2 rings appear to be circular and of identical diameter, within experimental error. The average height of strongly protruding (up) and weakly protruding (down) LH2 complexes above the plane of the lipid bilayer was 1.0 and 0.5 nm, respectively. This result is in agreement with the data of Scheuring *et al.* (17) on the same complex. From this we conclude that strongly protruded rings correspond to the periplasmic side of the LH2 complex. Without the use of single-particle averaging methods, we found that in some of the LH2 rings, the resolution was high enough to count the number of units per LH2 ring, which was nine.

FIG. 3. **LH2 crystals displaying three types of periodicity.** *A*, type A (zigzag): frame size, 200 × 200 nm²; full gray-scale, 1.8 nm. *B*, type B (rectangular): frame size, 200 × 200 nm²; full gray-scale, 2.4 nm. *C*, type C (disordered): frame size, 200 × 200 nm²; full gray-scale, 4.8 nm. *D*, an LH2 crystal displaying the co-existence of all three types of periodicity: frame size, 500 × 500 nm²; full gray-scale, 10 nm.

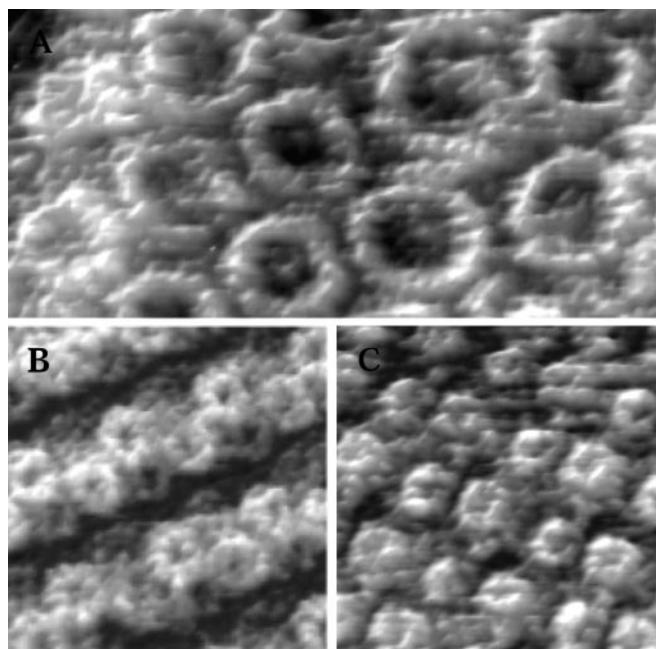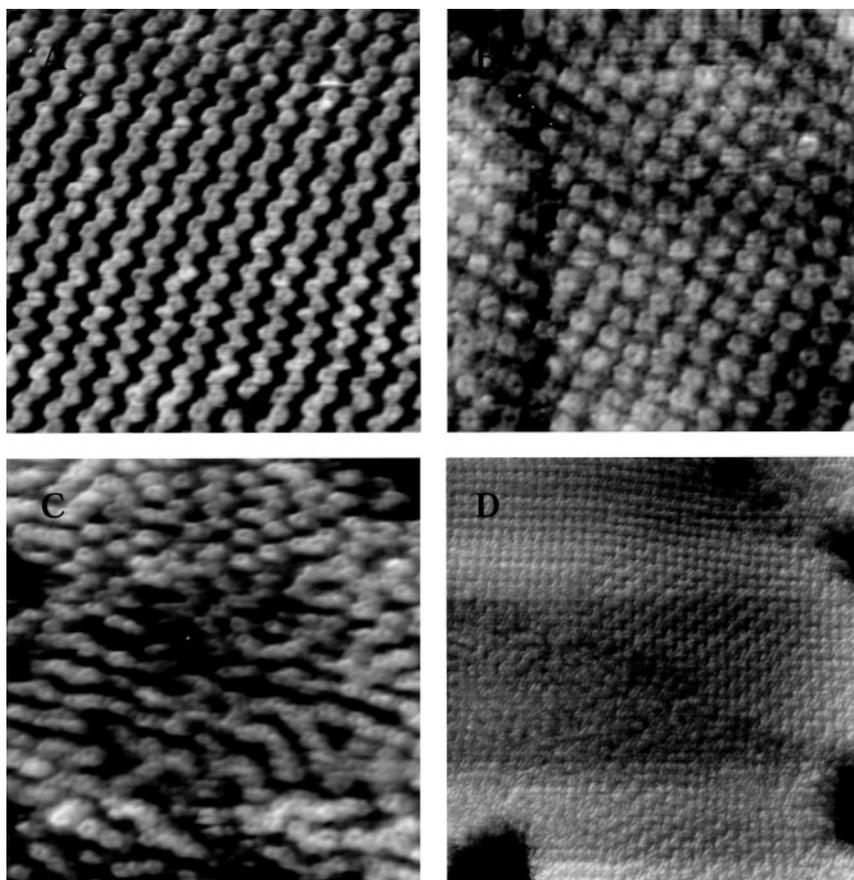FIG. 4. **High magnification topographs of LH1 and LH2 complexes.** *A*, LH1 rings (disordered area): frame size, 35 × 70 nm²; full gray-scale, 1.8 nm. *B*, LH2 rings (type A): frame size, 50 × 50 nm²; full gray-scale, 1.7 nm. *C*, LH2 rings (type B): frame size, 50 × 50 nm²; full gray-scale, 2 nm.

A Variety in Shapes, Sizes, and Conformation for LH1 Complexes—The variety of types of LH1 complex imaged by AFM could be observed from our analysis of ~300 individual LH1 complexes from ~10 different membrane patches. An overview of the variation in LH1 complexes is represented in Fig. 5. Circles (Fig. 5, *A–C*), polygonal rings (Fig. 5*D*), open rings (Fig.

5*E*), ellipses (Fig. 5, *F–H*), and more anomalous structures such as arcs (Fig. 5, *I* and *J*) were all observed. Polygonal rings are deformed rings, in which circular or elliptical ring architectures were considerably distorted. The ellipses and circles formed the two major groups, comprising 41 and 35% of the total number of complexes, respectively. Polygonal and open rings were observed less frequently, at 19 and 5%, respectively.

The differing ring sizes observed for LH1 had outer diameters of 11.6 ± 0.5 nm, 12.6 ± 0.5 nm, and 14.5 ± 0.8 nm, which are hereafter referred to as small, medium, and large. In the circular LH1 rings, the percentage of small rings (Fig. 5*A*) was 14%, medium rings (Fig. 5*B*) were 64%, and large rings (Fig. 5*C*) were 22%. Using the known size of the $\alpha\beta$-protomer, we suggest that the small rings contain 15 subunits, the medium contain 16, and the large contain 18 subunits. For ellipses, the occurrence of small, medium, and large (Fig. 5, *F–H*) was 24, 45, and 31%, respectively. The circularity of some of the LH1 complexes was confirmed by the practically equal diameters for two orthogonal directions. For the elliptical complexes, the ratio between short (*b*) and long (*a*) axes was found to vary slightly for different sizes: small ellipses, $b/a = 0.75$; medium and large ellipses, $b/a = 0.8$.

Table II in the supplemental material details other parameters that were measured for LH1 complexes. The height of weakly protruded LH1 rings above the lipid bilayer was 0.8 nm, which is similar to the height of empty LH1 rings on the periplasmic side for the *B. viridis* complex (19). The height of stronger protrusions of the LH1 complexes observed here and ascribed to the cytoplasmic face of the complex was 1.4 nm. The inner diameters of cytoplasmic and periplasmic faces of the small rings were 6.1 and 6.6 nm, respectively, medium rings were 6.5 and 7.3 nm, respectively, and large rings were 7.6 and 9 nm, respectively. Thus, in each case the inner diameter of the strongly protruding cytoplasmic surface of the LH1 rings is
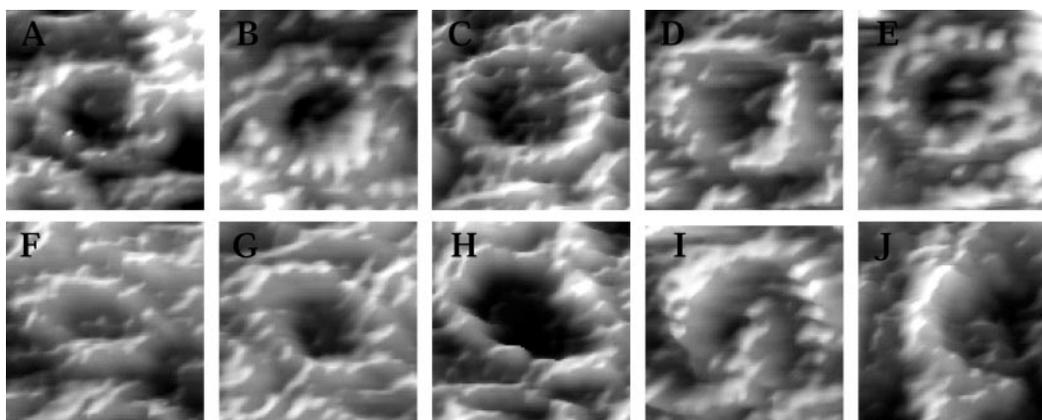
FIG. 5. **An overview of LH1 complexes, displaying the wide variation in shapes and sizes.** All 10 images have an image size of 18×18 nm. *A*, small circular. Percentage of total = 6%. Dimensions = 11.6 ± 0.5 nm, $n = 17$. *B*, medium circular. Percentage of total = 22%. Dimensions = 12.6 ± 0.5 nm, $n = 66$. *C*, large circular. Percentage of total = 7%. Dimensions = 14.5 ± 0.8 nm, $n = 23$. *D*, polygonal. Percentage of total = 19%. Dimensions, n/a; $n = 57$. *E*, open. Percentage of total = 5%. Dimensions = 12.7 ± 1.3 nm, $n = 17$. *F*, small elliptical. Percentage of total = 10%. Dimensions = $13.3 \, (\pm 1.1) \times 10.0 \, (\pm 1.1)$ nm, $n = 30$. *G*, medium elliptical. Percentage of total = 18%. Dimensions = $13.8 \, (\pm 1.2) \times 10.9 \, (\pm 1.2)$ nm, $n = 55$. *H*, large elliptical. Percentage of total = 13%. Dimensions = $14.4 \, (\pm 1.1) \times 11.4 \, (\pm 1.1)$ nm, $n = 39$. *I*, two intersecting arcs. *J*, single arc.

noticeably smaller than that of the weakly protruding periplasmic surface.

DISCUSSION

The flexibility, which has been suggested to be a functionally essential property of the LH1 complex, would require a dynamic series of conformations *in vivo*. We have used AFM to examine a population of LH1 molecules in a membrane environment at room temperature. Our work highlights the extraordinary variety of shapes and sizes exhibited by the isolated LH1 complex. This variety has not been visualized directly before by AFM, because previous studies have concentrated on the RC-LH1 complex, either in native membranes of *B. viridis* (19) or in two-dimensional crystals formed from the *R. rubrum* (20) and the *R. sphaeroides* RC-LH1-PufX complexes (6, 15). Ketelaars *et al.* (25) also noted that only 30% of the single RC-LH1 complexes of *R. acidophila* that they analyzed showed a spectrum consistent with a circular structure; the remainder were interpreted as either rings deformed in a C2 manner or incomplete rings.

AFM images were recorded by using tapping-mode imaging in liquid and by applying the lowest force possible. Previous AFM studies of bacterial LH complexes (16–19) employed contact-mode AFM, so it was important to establish at the outset that tapping-mode AFM is also effective. A comparison of contact- and tapping-mode AFM concluded that the former method tends to offer superior resolution, but that tapping-mode AFM, in which the tip touches the sample only at the end of a downward movement, is capable of imaging without detectable deformation of polypeptide domains (26).

It is likely that the presence of the RC inside the LH1 ring greatly restricts the range of conformations possible for LH1, necessitating removal of the RC, in this case by genetic means, to avoid accomplishing RC removal by employing detergent treatments. It should be stressed that the particular LH1-only strain used in this study did not contain the *pufX* gene, and thus the complex studied here is analogous to the LH1 complex from *R. rubrum* or *B. viridis*. Attempts were made to form ordered two-dimensional sheets reconstituted from monomeric LH1-only complexes; such crystals have already been reported (3) with sufficient order to be analyzed by negative-stain EM. However, it seems to be difficult to form very highly ordered two-dimensional sheets from LH1-only complexes. For example, there is evidence from transmission EM that the LH1-only strain of *B. viridis* produces membranes that are much more disordered than for the wild type containing the RC-LH1 com-

plex (27). The AFM images of LH1 arrays in Figs. 1 and 2 illustrate the inherent difficulties of reconstituting lattices with a high degree of order, because the isolated LH1 exhibits heterogeneity in both ring size and conformation. Although this is a disadvantage for crystallographic approaches, or any method that employs averaging procedures, it provides fascinating material for analysis by AFM.

It is surprising that even in the well ordered regions of the two-dimensional crystals of LH1-only complexes, there is apparently little tendency to aggregate in the alternating up-down-up arrangement often seen for LH2 and RC-LH1 complexes (3, 4, 17, 20). It is possible that this mode of packing arises from small differences in diameters of these complexes at the cytoplasmic and periplasmic faces, coupled with a certain amount of rigidity. Together, these might favor alternating associations in a two-dimensional lattice. The obvious flexibility of LH1 seen in the gallery of images in Fig. 5 might preclude any such up-down lattice and may explain the preponderance of one topology in our crystals.

Structural Basis for Variations in Size and Shape of the LH1 Complex and Comparison with the LH2 Complex—We have examined three different crystal forms and can find no overt variations in either size or shape for the LH2 complex. Clearly, there must be substantial differences between the protein architectures of LH1 and LH2 which are not apparent from a superficial examination of the primary sequences. We suggest that the one crucial difference between these complexes is the arrangement of H-bonds between the C-terminal regions of LH complexes and the C2 acetyl carbonyls of the bound Bchls. As already noted (28), a combination of resonance Raman and mutagenesis approaches has shown that a network of H-bonds stabilizes each $\alpha_1\beta_1$Bchl$_2$ unit within LH1, so that the four possible H-bonds to each pair of Bchls are donated by the α and β polypeptides that bind the same Bchls (23, 29, 30). Thus, these four H-bonds are internal to the $\alpha_1\beta_1$Bchl$_2$ unit and provide a significant driving force to stabilize this complex (31). In contrast, the H-bonding arrangements for the nonameric LH2 complexes from *R. sphaeroides* and *R. acidophila* each involve one H-bond internal to an $\alpha\beta$ pair of polypeptides, but with the other bond directed toward the neighboring $\alpha\beta$ pair. This difference is depicted in Fig. 6, which shows a portion of the ring of the *R. acidophila* complex (32) in Fig. 6*A* and schematically in 6*C*, and of the LH1 complex in Fig. 6*B*, modeled from EM, NMR, mutagenesis, and AFM data (20), and schematically in Fig. 6*D*. The effect of these differing arrange-
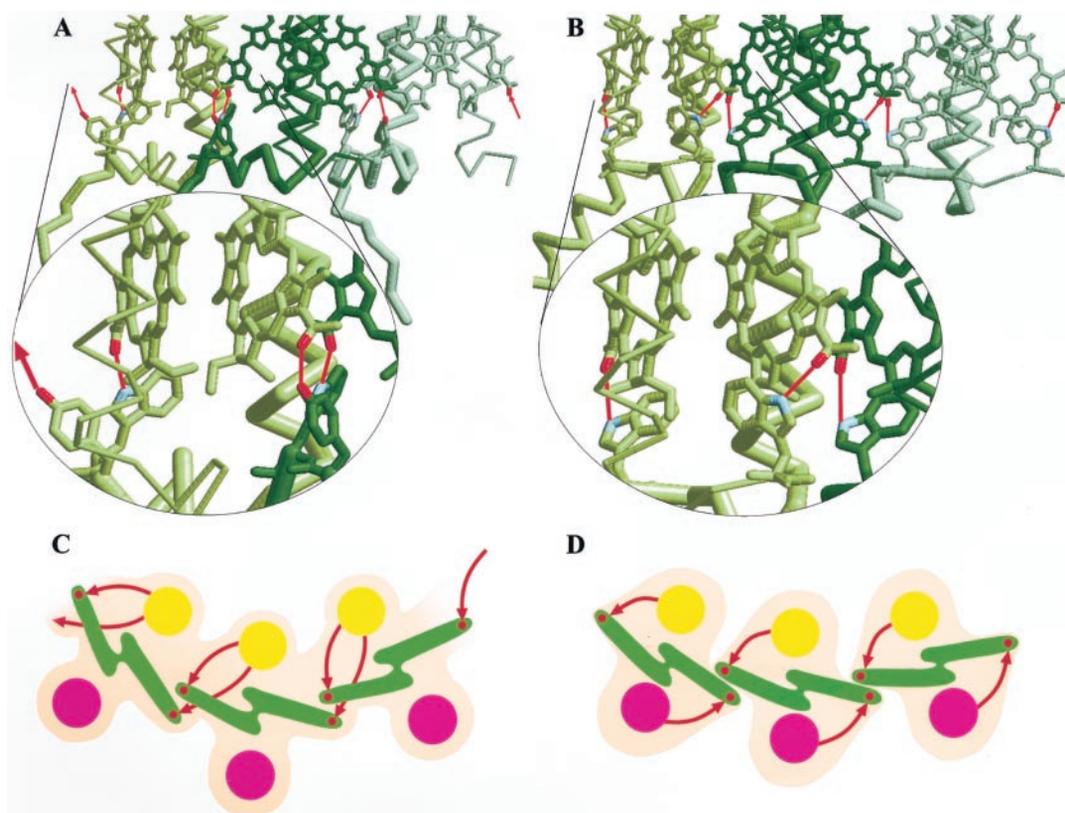
FIG. 6. **Diagram illustrating the differences in H-bonding between nonameric LH2 complexes (*A and C*) and 16-membered LH1 complexes (*B and D*).** This diagram shows the arrangement of H-bonds between the C-terminal regions of LH complexes and the C2 acetyl carbonyls of the bound Bchls. *A*, the H-bonding arrangement for the nonameric LH2 complexes from *R. sphaeroides* and *R. acidophila* involves one H-bond internal to each $\alpha\beta$ pair of polypeptides but with the other bond directed toward the neighboring $\alpha\beta$ pair (*C*). Each pair of LH polypeptides and their Bchls is color coded in a different shade of green. *B*, the H-bonding arrangement for the LH1 complex, with color coding as in *A*. The four possible H-bonds to each pair of Bchls are donated by the α and β polypeptides that bind the same Bchls. Thus, these four H-bonds are internal to the $\alpha_1\beta_1$Bchl$_2$ unit (*D*). *C*, a schematic representation of *A*, with the α polypeptide in *yellow*, the β polypeptide in *magenta*, Bchls in *green*, and the H-bonds denoted by *red arrows* showing the linkage between adjacent protomers. *D*, a schematic representation of *B* with colors as in *C*, showing the H-bonds confined to individual protomers, one from the α polypeptide and the other from the β polypeptide. The effect of these differing arrangements is that each $\alpha_1\beta_1$Bchl$_2$ unit within LH1 has a certain degree of autonomy within the complex, when compared with LH2.

ments is that each $\alpha_1\beta_1$Bchl$_2$ unit within LH1 has a certain degree of autonomy within the complex. This is depicted schematically by showing separate $\alpha_1\beta_1$Bchl$_2$ units in Fig. 6*D*, and a continuity of inter-linked H-bonds in Fig. 6*C*. This difference is borne out by the facts that LH1 can be readily dissembled into individual $\alpha_1\beta_1$Bchl$_2$ units, often termed B820 (33), and that it can also be fractionated into a series of LH1 oligomers that vary in size from $(\alpha\beta)_{2-3}$ to $(\alpha\beta)_{10-11}$ (34, 35). Neither of these types of subdivision of a nonameric LH2 complex has been reported, although the octomeric LH2 of *Rhodospirillum molischianum* has been successfully dissociated into B820 subunits (36). Fig. 6 provides a rationale for the *R. molischianum* LH2 dissociation, because its H-bonding arrangement resembles that of LH1 (37). In the light of these differences between LH1 and nonameric LH2 complexes, it is easier to understand why LH2 displays no variation in either its size or shape detectable by AFM, and why LH1 behaves as a loosely connected series of $\alpha_1\beta_1$Bchl$_2$ units, capable of forming the circular, elliptical, polygonal, and open rings represented in Fig. 5.

Biological Significance of the Flexibility and Deformability of LH1—The RC-LH1 complex is already known to adopt both circular and elliptical conformations, as seen in the EM projection maps (4) and more recently in three-dimensional crystals (5). This implied flexibility of the LH1 complex was suggested to be important for its function, by allowing the export of quinol formed as a result of reaction center photochemistry (4). AFM topographs of the membrane-bound *B. viridis* RC-LH1 complex demonstrated a similar ellipticity, which altered to a circular

shape upon removal of the RC (19). The shapes of the LH1-only complex in Fig. 5 reveal a much more flexible structure than was suspected previously. It was not clear why an ability to slightly deform LH1 of *B. viridis* or *R. rubrum* into circular or elliptical shapes would, by itself, allow the passage of quinol from the enclosed RC to the external quinone pool. Our demonstration that the linkage between adjacent $\alpha_1\beta_1$Bchl$_2$ units is flexible and also even breakable at room temperature in a detergent-free membrane bilayer provides a rationale for the transient opening and closing of LH1 units adjoining the Q$_B$ site of the RC. The existence of open rings and arcs in our samples serves to illustrate this point, because it shows that LH1 can indeed form stable but interrupted oligomers, as was proposed by Westerhuis *et al.* (34) on the basis of lithium dodecyl sulfate-solubilized LH1-only complexes. In addition, this temporary uncoupling is compatible with the presence of the PufX polypeptide, which interrupts the continuity of the ring of Bchls but effectively becomes a part of the LH1 ring system by associating closely with the LH1α polypeptide (38), perhaps providing a weak link. AFM topographs of LH1+PufX two-dimensional crystals of *R. sphaeroides* also show open rings, though at the current resolution we cannot determine whether these occur adjacent to PufX.[2]

Origin and Significance of Variable Ring Sizes for LH1— None of the above would necessarily lead to an observation of

---

[2] S. Bahatyrova, J. D. Olsen, C. N. Hunter, C. Otto, unpublished data.

different ring sizes, yet the data clearly show the existence of open rings as well as a variety of ring diameters. It might be argued that the different ring sizes, and indeed the open rings, are merely artifacts of the purification procedure. We do not believe that the complexes undergo radical dissociation/re-association during our preparation, as there is no sign of a peak at either 777 or 820 nm in the post-purification material that was used for the two-dimensional crystallization trials (see Fig. 1 in supplemental material). The conditions that are known to dissociate LH1 of *R. sphaeroides* into B820 subunits necessitate the use of either a carotenoidless mutant LH1 or the extraction of lyophilized chromatophores with petroleum ether to obtain efficient dissociation of the complex (39). We suggest that the presence of native carotenoids in our complexes protects them against the concentration of β-OG used; indeed Scheuring *et al.* (15) used 3% β-OG to isolate and purify dimeric core complexes of *R. sphaeroides*, indicating that delicate higher orders of organization are preserved, even at this high concentration of β-OG.

The dimensions of the large LH1-only ring measured by AFM would be compatible with enclosing an RC complex and there may be no imperative for the assembly of $\alpha_{16}\beta_{16}$Bchl$_{32}$ units. A recent AFM analysis of reconstituted two-dimensional crystals of *R. sphaeroides* RC-LH1-PufX complexes demonstrated the existence of a small proportion of larger diameter (13.4 nm) rings (6). The AFM study of Scheuring *et al.* (19) on native membranes of *B. viridis* reported 16-fold rings, although the data processing could have masked the presence of other ring sizes. Currently it is not known how the assembly system senses when the correctly sized ring is nearing completion and how it halts this process. It is known that LH1 can assemble *in vitro* from its constituent $\alpha_1\beta_1$Bchl$_2$ units (33), but currently the mode of *in vivo* assembly of LH1 is not known, although it has been shown that there is an assembly factor for the RC-LH1 complex (40, 41). We have observed variability in LH1 aggregation in membranes where both PufX and the RC are absent; thus, one or both of these components might be an important factor in determining the LH1 ring size of *R. sphaeroides*. Perhaps the absence of the RC complex deprives the assembly system of a guide or template on which to assemble LH1, and in its absence, some variation in oligomerization takes place. However, only *in situ* imaging of the membranes of the LH1-only mutant will unequivocally decide this issue.

To conclude and summarize, this paper has used AFM to demonstrate large variations from molecule to molecule in the LH1 light harvesting complex, in terms of both shape and size. Freed from enclosing the RC, the inherent flexibility and lack of structural coherence of this complex become apparent. In particular, the existence of open rings and arcs provides a direct visualization of consequences of the relatively weak associations that govern the association of the $\alpha_1\beta_1$Bchl$_2$ protomers comprising the LH1 complex. These associations, which are known to be significantly different for the readily dissociated LH1 complex and the stable nonameric LH2 complex, are suggested to arise from the H-bonding patterns that stabilize binding of the Bchls to the LH polypeptides. This relative instability, exaggerated here by the genetic removal of the RC, forms the basis for a dynamic separation of individual $\alpha_1\beta_1$Bchl$_2$ protomers, thus allowing passage of quinol from the RC to the quinone pool prior to reduction of the cytochrome bc_1 complex.

REFERENCES

1. Blankenship, R. E. (2002) in *Molecular Mechanisms of Photosynthesis*, pp. 61–82, Blackwell Science Ltd., Oxford
2. McDermott, G., Prince, S. M., Freer, A. A., Hawthornthwaite-Lawless, A. M., Papiz, M. Z., Cogdell, R. J., and Isaacs, N. W. (1995) *Nature* **374,** 517–521
3. Walz, T., Jamieson, S. J., Bowers, C. M., Bullough, P. A., and Hunter, C. N. (1998) *J. Mol. Biol.* **282,** 833–845
4. Jamieson, S. J., Wang, P., Qian, P., Kirkland, J. Y., Conroy, M. J., Hunter, C. N., and Bullough, P. A. (2002) *EMBO J.* **21,** 3927–3935
5. Roszak, A. W., Howard, T. D., Southall, J., Gardiner, A. T., Law, C. J., Isaacs, N. W., and Cogdell, R. J. (2003) *Science* **302,** 1969–1972
6. Siebert, C. A., Qian, P., Fotiadis, D., Engel, A., Hunter, C. N., and Bullough, P. A. (2004) *EMBO J.* **23,** 690–700
7. Farchaus, J. W., and Oesterhelt, D. (1989) *EMBO J.* **8,** 47–54
8. Farchaus, J. W., Barz, W. P., Grunberg, H., and Oesterhelt, D. (1992) *EMBO J.* **11,** 2779–2788
9. Lilburn, T. G., and Beatty, J. T. (1992) *FEMS Microbiol. Lett.* **100,** 155–159
10. Barz, W. P., Vermeglio, A., Francia, F., Venturoli, G., Melandri, B. A., and Oesterhelt, D. (1995) *Biochemistry* **34,** 15248–15258
11. Cogdell, R. J., Fyfe, P. K., Barrett, S. J., Prince, S. M., Freer, A. A., Isaacs, N. W., McGlynn, P., and Hunter, C. N. (1996) *Photosynth. Res.* **48,** 55–63
12. McGlynn, P., Hunter, C. N., and Jones, M. R. (1994) *FEBS Lett.* **349,** 349–353
13. Frese, R. N., Olsen, J. D., Branvall, R., Westerhuis, W. H., Hunter, C. N., and van Grondelle, R. (2000) *Proc. Natl. Acad. Sci. U. S. A.* **97,** 5197–5202
14. Francia, F., Wang, J., Venturoli, G., Melandri, B. A., Barz, W. P., and Oesterhelt, D. (1999) *Biochemistry* **38,** 6834–6845
15. Scheuring, S., Francia, F., Busselez, J., Melandri, B. A., Rigaud, J. L., and Levy, D. (2004) *J. Biol. Chem.* **279,** 3620–3626
16. Scheuring, S., Reiss-Husson, F., Engel, A., Rigaud, J. L., and Ranck, J. L. (2001) *EMBO J.* **20,** 3029–3035
17. Scheuring, S., Seguin, J., Marco, S., Levy, D., Breyton, C., Robert, B., and Rigaud, J. L. (2003) *J. Mol. Biol.* **325,** 569–580
18. Stamouli, A., Kafi, S., Klein, D. C. G., Oosterkamp, T. H., Frenken, J. W. M., Cogdell, R. J., and Aartsma, T. J. (2003) *Biophys. J.* **84,** 2483–2491
19. Scheuring, S., Seguin, J., Marco, S., Levy, D., Robert, B., and Rigaud, J. L. (2003) *Proc. Natl. Acad. Sci. U. S. A.* **100,** 1690–1693
20. Fotiadis, D., Qian, P., Pilippsen, A., Bullough, P. A., Engel, A., and Hunter, C. N. (2004) *J. Biol. Chem.* **279,** 2063–2068
21. Jones, M. R., Fowler, G. J. S., Gibson, L. C. D., Grief, G. G., Olsen, J. D., Crielaard, W., and Hunter, C. N. (1992) *Mol. Microbiol.* **6,** 1173–1184
22. Simon, R., Priefer, U., and Pühler, A. (1983) *Bio/Technology* **1,** 784–791
23. Olsen, J. D., Sockalingum, G. D., Robert, B., and Hunter, C. N. (1994) *Proc. Natl. Acad. Sci. U. S. A.* **91,** 7124–7128
24. van der Werf, K. O., Putman, C. A. J., de Grooth, B. G., Segerink, F. B., Schipper, E. H., van Hulst, N. F., and Greve, J. (1993) *Rev. Sci. Instrum.* **64,** 2892–2897
25. Ketelaars, M., Hofmann, C., Kohler, J., Howard, T. D., Cogdell, R. J., Schmidt, J., and Aartsma, T. J. (2002) *Biophys. J.* **83,** 1701–1715
26. Moller, C., Allen, M., Elings, V., Engel, A., and Muller, D. J. (1999) *Biophys. J.* **77,** 1150–1158
27. Ostafin, A. E., Ponomarenko, N. S., Popva, J. A., Jager, M., Bylina, E. J., and Norris, J. R. (2003) *Photosynth. Res.* **77,** 53–68
28. Pugh, R. J., McGlynn, P., Jones, M. R., and Hunter, C. N. (1998) *Biochim. Biophys. Acta* **1366,** 301–316
29. Olsen, J. D., Sturgis, J. N., Westerhuis, W. H., Fowler, G. J. S., Hunter, C. N., and Robert, B. (1997) *Biochemistry* **36,** 12625–12632
30. Sturgis, J. N., Olsen, J. D., Robert, B., and Hunter, C. N. (1997) *Biochemistry* **36,** 2772–2778
31. Davis, C. M., Bustamante, P. L., Todd, J. B., Parkes-Loach, P. S., McGlynn, P., Olsen, J. D., McMaster, L., Hunter, C. N., and Loach, P. A. (1997) *Biochemistry* **36,** 3671–3679
32. Papiz, M., Prince, S. M., Howard, T., Cogdell, R. J., and Isaacs, N. W. (2003) *J. Mol. Biol.* **326,** 1523–1538
33. Miller, J. F., Hinchigeri, S. B., Parkes-Loach, P. S., Callahan, P. M., Sprinkle, J. R., Riccobono, J. R., and Loach, P. A. (1987) *Biochemistry* **26,** 5055–5062
34. Westerhuis, W. H. J., Sturgis, J. N., Ratcliffe, E. C., Hunter, C. N., and Niederman, R. A. (2002) *Biochemistry* **41,** 8698–8707
35. Westerhuis, W. H. J., Hunter, C. N., van Grondelle, R., and Niederman, R. A. (1999) *J. Phys. Chem. B* **103,** 7733–7742
36. Todd, J. B., Parkes-Loach, P. S., Leykam, J. F., and Loach, P. A. (1998) *Biochemistry* **37,** 17458–17468
37. Germeroth, L., Lottspeich, F., Robert, B., and Michel, H. (1993) *Biochemistry* **32,** 5615–5621
38. Recchia, P. A., Davis, C. M., Lilburn, T. G., Beatty, J. T., Parkes-Loach, P. S., Hunter, C. N., and Loach, P. A. (1998) *Biochemistry* **37,** 11055–11063
39. Chang, M. C., Meyer, L., and Loach, P. A. (1990) *Photochem. Photobiol.* **52,** 873–881
40. Young, C. S., Reyes, R. C., and Beatty, J. T. (1998) *J. Bacteriol.* **180,** 1759–1765
41. Young, C. S., and Beatty, J. T. (1998) *J. Bacteriol.* **180,** 4742–4745